Al-Nahrain Journal for Engineering Sciences

Al-Nahrain J. Eng. Sci. 29(2) 198-208, 2026
Original Article

Behavior of R.C Slab-Column Connections with Square and Circular Columns under Gravity and Lateral Cyclic Loading Conditions

Abathar M. Al-Yaseri [1] and Laith Kh. Al-Hadithy [2] ●

1Civil Engineering Department, Kerbala University, Karbala, Iraq

2 Department of Civil Engineering, College of Engineering, Al -Nahrain University, Baghdad, Iraq

●These authors contributed equally to this work

DOI: https://www.doi.org/10.29194/NJES.29020198

Received: April 30, 2025 **Revised:** June 2, 2025 **Accepted:** July 13, 2025 **Published:** June 20, 2026

Abstract

This experimental investigation evaluates the structural behavior of reinforced concrete slab-column connections incorporating columns with square and circular cross-sectional geometries under gravity and lateral cyclic loading. Four interior slab-column specimens were designed, fabricated, and tested, with identical slab dimensions of 1050×1050×80 mm and a column height of 500 mm. The circular columns were intended to have an equivalent second moment of inertia to the square column, ensuring a fair comparison of geometric effects. One specimen identified as SC-G, incorporating a square column, was tested under a progressively increasing vertical load to determine its maximum gravity load-bearing capacity. The remaining three specimens SC-2 with a square tied column, SC-9 with a circular spirally-reinforced column, and SC-10 with a circular column incorporating a column capital were tested under a constant gravity load equivalent to 60% of SC-G's ultimate capacity (75 kN), combined with a lateral displacement protocol conforming to ACI 374 guidelines. Results indicated that the shape of the column (circular) and reinforcement (spiral) in SC-9 produces a comparatively higher ultimate load, stiffness, and ductility than SC-2 of the square column and tied reinforcement. The ultimate lateral load increase was +13.3%, -26.1%. Circular spiral columns with column capital in slab-column connections led to a noticeable rise in ultimate lateral load by about +62%, -80%. It was also shown that incorporating a column capital in SC-10 significantly enhanced the punching shear resistance and energy dissipation capacity. Circular columns demonstrated more stable hysteretic behavior and improved ductility compared to the square column specimen.

Keywords: *Slab-Column Connections, Gravity load, Lateral Cyclic Loading, Circular Columns.*

Corresponding author: Provide the corresponding author information and publisher here. E-mail address: abathar.m@uokerbala.edu.iq

1. Introduction

Flat plate systems are widely employed in modern reinforced concrete (RC) buildings due to their architectural flexibility, reduced story heights, simplified formwork, and enhanced serviceability. However, despite their benefits, these systems remain highly susceptible to punching shear failure at the slab-column interface, particularly under high vertical loads or seismic excitation. The brittle and sudden nature of punching shear failure can lead to progressive collapse, as has been documented in multiple past structural failures worldwide [1].

The slab-column region, inherently less stiff and ductile than traditional beam-column frames, is especially susceptible to combined vertical gravity loads and lateral cyclic displacements, such as those induced by earthquakes. Evidence from experimental studies and seismic events such as the 1985 Mexico City and 1994 Northridge earthquakes has highlighted the vulnerability of flat plate systems lacking adequate detailing or shear reinforcement, often leading to significant structural damage or complete collapse. While shear reinforcement and structural enhancements such as drop panels and column capitals can improve performance, the influence of column geometry on the seismic behavior of slab-column joints remains a critical area warranting further investigation [2].

Flat plate systems are defined by their configuration, where floor slabs rest directly on columns without incorporating beams for intermediate support. They are widely favored in reinforced concrete construction due to their architectural flexibility, efficiency, and reduced story heights. However, a critical vulnerability of these systems lies in the slab-column connections, where punching shear failure, an abrupt and brittle failure mode, can initiate catastrophic progressive collapse. This concern becomes significantly pronounced when such systems are subjected to seismic loading, where lateral cyclic displacements are superimposed on existing gravity loads [3].

The punching shear phenomenon arises from high stress concentrations around the slab-column interface, often leading to truncated conical or pyramidal failure surfaces [4]. Several factors affect this structural behavior, such as the compressive strength of concrete, the ratio of flexural reinforcement, the thickness of the slab, the dimensions of the column, and whether shear reinforcement is provided. While several design codes, such as ACI 318-19 [5], Eurocode 2[6], CSA A23.3-19 [7], and JSCE 2007[8], offer guidance on punching shear capacity, notable differences exist in their predictive models, particularly in critical section definitions and strength provisions.

A wide range of experimental research has focused on evaluating how these parameters influence punching shear strength. Findings consistently indicate that higher concrete compressive strength and increased flexural reinforcement ratios contribute to greater punching resistance and improved deformation capacity in slab-column connections. Similarly, incorporating shear reinforcement such as stirrups, headed studs, or steel fibers has substantially enhanced ductility and energy dissipation, particularly when subjected to cyclic lateral loading [9].

The influence of seismic loading on slab-column connections has been a growing research focus. Cyclic lateral displacements, representing earthquake effects, cause stiffness degradation and increase vulnerability to brittle shear failure [10,11]. Experimental investigations have highlighted those parameters such as column geometry, reinforcement detailing, and the presence of column capitals play a critical role in mitigating seismic-induced distress. In particular, circular columns have shown improved stress distribution and rotational capacity compared to square columns, potentially delaying the onset of shear failure. Employing column capitals has also proven effective in extending the critical punching shear perimeter, thereby improving the load-bearing capacity of the connection [12]. Although considerable research has addressed punching shear behavior in flat plate systems, there remains a scarcity of studies that directly compare the seismic performance of slab-column connections featuring different column shapes but equivalent flexural stiffness. Furthermore, the combined effect of gravity and lateral cyclic loading on the behavior of such connections remains insufficiently addressed in current literature, especially in configurations incorporating circular columns with capitals [13].

Truong et al. (2022) experimentally investigated the punching shear strength of interior concrete slab-column connections reinforced with Fiber Reinforced Polymer (FRP) flexural and shear reinforcement. This study demonstrated that FRP reinforcement, applied for flexure and shear, significantly enhances the punching shear resistance and ductility of slab-column connections. It was also highlighted that the benefits of using FRP as an alternative to traditional steel reinforcement, particularly in enhancing seismic performance and delaying brittle failure modes [14].

Sarhan et al. (2017) presented an experimental study examining the punching shear resistance of high-strength concrete flat slabs reinforced with glass fiber-reinforced polymer (GFRP) bars. The results showed that GFRP reinforcement enhances the slab's punching shear capacity compared to conventional steel reinforcement, albeit with different failure mechanisms and strain characteristics. The study emphasizes the effectiveness of GFRP as a viable reinforcement option, particularly in environments susceptible to corrosion [15]. Yousif et al. (2017) conducted a numerical investigation using the finite element method (FEM) to analyze the punching strength of glass fiber-reinforced polymer (GFRP) reinforced concrete slab-column connections with various opening configurations. The study highlighted that openings significantly reduce the punching capacity of such connections; however, GFRP reinforcement can partially compensate for this reduction by providing improved post-cracking behavior [16]. Zhou and Hrynyk (2024) conducted a finite element study to evaluate the punching shear capacity of post-tensioned precast concrete two-way slab-column connections under gravity and lateral loading. Their results showed that post-tensioning significantly improved punching shear resistance by enhancing the stress distribution and delaying cracking initiation. The study also revealed that using precast elements required careful attention to connection detailing to ensure adequate rotational capacity and ductility [17].

Jia and Chiang (2023) used ABAQUS finite element modeling to investigate the punching shear behavior of reinforced concrete mushroom slab-column connections. Their analysis demonstrated that flexural reinforcement and slab thickness substantially influenced the load-carrying capacity. The numerical models captured the development of critical cracking patterns, correlating well with experimental data. The study concluded that ABAQUS provides a reliable framework for predicting the punching shear failure mechanism in slab-column joints [18].

Babu and Thenmozhi (2021) conducted experimental tests and numerical simulations on concrete slabs incorporating sintered fly ash aggregates to study their punching shear capacity. Results indicated that using sintered fly ash aggregates led to a slight reduction in punching strength compared to conventional concrete; however, the difference was within acceptable design tolerances. Their finite element analysis validated the experimental findings, highlighting the potential of sustainable materials in reinforced concrete structures [19].

Rafiee et al. (2021) evaluated new seismic details for connecting post-tensioned flat slabs to steel columns using steel plates, vertical stiffeners, and bolts. Their experiments revealed that these details improved the ultimate lateral load capacity by up to 40% compared to traditional connections. The new configurations also demonstrated enhanced ductility and better energy dissipation, significantly delaying punching shear failure under lateral cyclic loading [20].

Rafiee and Marefat (2020) conducted experimental and numerical analyses of post-tensioned flat slab connections with edge steel columns, focusing on innovative seismic detailing. Results showed that the proposed details using steel plates and stiffeners enhanced the connections' ultimate lateral load capacity and energy dissipation by over 50% compared to conventional designs. The study confirmed that these details reduced the vulnerability to brittle punching shear failures during seismic events [21].

The novelty of this study is "comparing slab-column connections with square and circular columns under combined gravity and lateral cyclic loading,". The use of circular columns with spiral reinforcement and column capitals under seismic-like loading remains a scarcely addressed topic in current literature. The research gap was a lack of direct comparative experimental studies on the seismic performance of slab-column joints with equivalent stiffness but different column shapes, especially under realistic lateral cyclic loading and incorporating column capitals.

2. Research Objective

This study aims to experimentally evaluate the structural response of reinforced concrete slab-column connections incorporating different column shapes when subjected to the combined action of gravity and lateral cyclic loads, in light of the vulnerabilities of flat plate systems to punching shear failure, particularly under seismic excitations. This study aims to deepen the understanding of how column shape and detailing influence the overall connection performance.

3. Experimental Program

This experimental work aims to provide a comparative assessment of how column shape and capital detailing affect punching shear behavior, lateral resistance, energy dissipation, ductility, and failure mechanisms in RC flat-plate connections under realistic seismic loading scenarios. Figure 1 illustrates a comprehensive schematic diagram for the experimental program of this study.

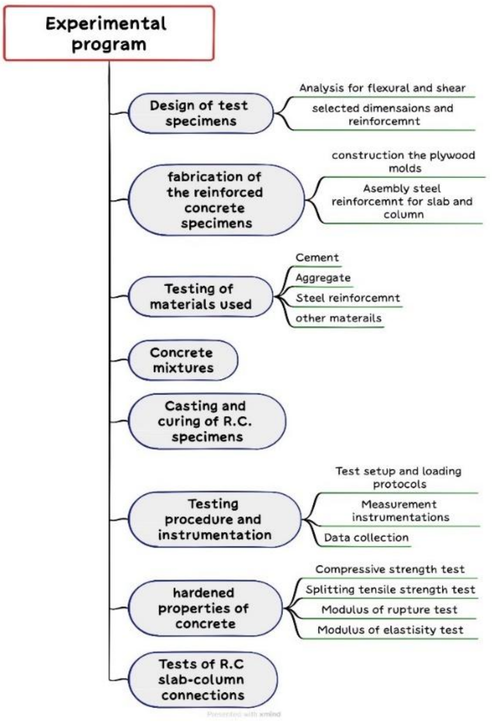

Figure 1. A Schematic Diagram of the Research Flowchart

3.1. Specimen Design and Description

Four 1:2.5-scale interior slab-column specimens were designed, cast, and tested. Specimen SC-G was exposed to a monotonic vertical load to establish its ultimate punching shear strength. The remaining three specimens (SC-2, SC-9, SC-10) were tested under a combination of a constant gravity load (75 kN, equivalent to 60% of SC-G's ultimate capacity) and the reversed lateral cyclic displacements following the ACI 374 loading protocol [22]. Each specimen consisted of a 1050×1050×80 mm slab and a 500 mm long column. SC-2 featured a square tied column (120×120 mm), SC-9 incorporated a circular spirally-reinforced column of equivalent flexural stiffness, and SC-10 had a similar circular column with an added column capital to enhance punching shear resistance. Flexural slab reinforcement consisted of 15 bars of 8 mm diameter in the tension zone and 7 bars in the compression zone in each direction. Columns were reinforced with eight longitudinal bars of 8 mm diameter and enclosed by 6 mm lateral ties at 55 mm spacing.

3.2. Specimen Geometry and Reinforcement Details:

All specimens shared identical geometric configurations. The columns and slabs were cast monolithically using normal-strength concrete with a cylinder compressive strength of 31.3 MPa, ensuring adequate bond and overall structural integrity. Slab dimensions (1050 × 1050 × 80) mm and column (120 × 120 × 500) mm. All the slabs were reinforced with two layers in each direction (with reinforcement ratio $\varrho=0.0125$ for the tension zone and $\varrho=0.006$ for the compression zone). In the slab reinforcement, ϕ8 mm steel bars were used. A longitudinal reinforcement for each column, eight ϕ8 mm bars (reinforcement ratio of 0.028) are symmetrically used (for uniform strength distribution in the structure). The confined reinforcement (ϕ6 mm ties at 55 mm center-to-center) ensured adequate confinement of these columns to prevent premature column failure. The slab and column reinforcements were designed for adequate flexural and shear capacity, to ensure punching shear failure was the failure mode. The style of Fig. 2 is so clear and concise that it gives the dimensions and reinforcement for the slab and column.

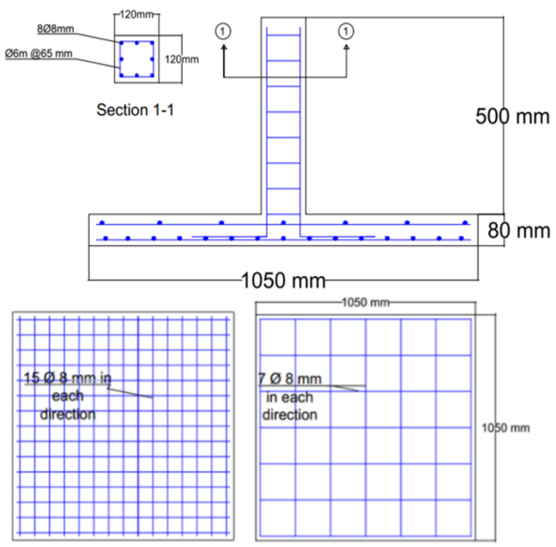

Figure 2. Dimensions and reinforcement details for the column and tested specimens

3.3. Properties of the Material Used

All specimens discussed in this paper were cast using a Normal Strength Concrete mixture (NSC). The concrete mix comprised Type V Portland cement, locally sourced natural sand, crushed gravel (maximum size 10 mm), and potable mixing water. The third generation of high-range water-reducing and superplasticizing admixtures has obtained specified compressive strength concrete with minimal water use. This type was produced by Sika (Sika® ViscoCrete®-180 GS, Sika company) [23] and was also used to improve workability without increasing water content. The mix proportions are illustrated in Table 1.

The properties of steel reinforcement bars were tested according to ASTM A615[24]. Bars ϕ8 mm were used to reinforce slabs and longitudinal column reinforcement. For tied and spiral reinforcement, ϕ6 mm was used. The test results of these bars are included in Table 2. Test results of coarse and fine aggregate are presented in Tables 3 and 4.

Table 1. Mix Proportions of the Concrete Mixture Used in (kg/m^3).

Cement	Fine aggregate	Coarse aggregate	water	Super plasticizer
350	870	1050	165	3.5

Table 2. Test Results of Steel Reinforcement Bar Used

D (mm)	fy (MPa)	fu (MPa)	Elongation (%)	Grade
6	530.2	715.6	11.9	G75
8	456.1	503.4	12.4	G40

***D:** bar diameter of steel reinforcement, ***fy:** Yield stress of steel*, ***fu:** ultimate stress of steel reinforcement*

Table 3. Grading and Chemical Tests of Ordinary Coarse Aggregate

Test	Sieve size (mm)	Passing %	Limits of the Iraqi Specification NO.45/2019 [25]
Grading	14	/	100
	9.5	96.4	85-100
	4.75	3.6	0-25
	2.36	0.42	0-5
Sulfate		0.07	0.1% (max)

Table 4. Grading and chemical tests of fine aggregate

Test	Sieve size (mm)	% Passing	Limits of the Iraqi Specification NO.45/2019 (Zone 2) [25]
Grading	4.75	98	90-100
	2.36	77	75-100
	1.18	64	55-90
	0.60	40	35-59
	0.30	10	8-30
	0.15	3	0-10
Sulfate		0.2	0.5 (max)

3.3. Casting and Curing Stages of Reinforced Concrete Specimens

The casting and curing procedures were carefully executed to ensure consistency and quality across all specimens. Four reinforced concrete slab-column connection specimens were fabricated for testing. They were fabricated using standardized molds made of 12 mm-thick plywood, dimensioned precisely to the target slab size of 1050×1050×80 mm and column height of 500 mm. The molds were firmly assembled using steel screws and treated with form-release oil to facilitate easy demolding after curing.

Before casting, pre-assembled reinforcement cages for both slabs and columns were securely tied and accurately positioned within the molds using plastic spacers to maintain the required concrete cover of 15 mm for both slab and column reinforcements. Dowels connecting the slab and column reinforcement were carefully aligned to ensure adequate bond and monolithic behavior at the interface.

Concrete placement was carried out in a single continuous pour using a mechanical vibrator to eliminate air pockets and ensure homogeneous compaction. Immediately after casting, the surface of each specimen was covered with nylon sheeting to minimize moisture loss due to evaporation. After an initial setting, all specimens were subjected to water curing for 14 days to achieve the required hydration and strength development. The duration of 14 days is based on relevant standards and guidance for attaining sufficient hydration and strength development in concrete. According to ACI 308R-16 ("Guide to External Curing of Concrete") [26], while 7 days is generally considered the minimum for moist curing, an extended period of 14 days is recommended to ensure adequate strength gain and durability, especially in cases where environmental conditions or material properties might influence hydration.

Furthermore, our mix design used Portland cement with a typical water-cement ratio, which achieves more than 90% of its 28-day strength after 14 days of water curing, consistent with widely accepted hydration curves. But the test was conducted after 28 days with the desired and designed compressive strength. This consistent casting and curing methodology helped maintain uniformity across the test specimens, minimizing variability in material properties and ensuring reliable performance comparisons under subsequent loading conditions. Figure 3 shows the stages of casting and curing of the reinforced concrete specimens.

Figure 3. Casting and curing processes of R.C specimens

3.4. Test Setup and Instrumentation

A concentric vertical load was imposed on specimen SC-G with an increasing magnitude until failure occurred. A similar test was carried out for the other four specimens, under constant gravity (75 kN, approximately 60% of the ultimate capacity of SC-G), applied through a vertical hydraulic jack. According to a cyclic displacement protocol, they applied a cyclic lateral displacement at the top of the column. The following instruments were used to monitor the response of specimens during testing:

- Two load cells for measuring applied vertical gravity and lateral cyclic loads.
- Linear Variable Displacement Transducers (LVDTs) were strategically positioned at various points to monitor slab deflections and column displacements.
- Column and slab reinforcement strain gauges to evaluate strain distribution.

All specimens rested over a supported steel frame in which support is provided along all four edges, and the corners were restrained against upward uplift. The lateral displacement in the slab was constrained to align with the direction of the applied lateral force. The specimens were cleaned before testing, and all sides were painted white to indicate crack propagation. Figure 4 shows the testing setup and the instrumentation.

Figure 4. Test setup and components of testing, 1) Steel frame 2) Vertical actuator 3) Vertical load cell 4) Lateral actuator 5) Lateral load cell 6) Support of the specimens

3.5. Types of Loading

3.5.1 Gravity Loading

Specimen SC-G was tested under monotonically increasing vertical load to establish its ultimate punching capacity. The load was applied via a 1000 kN hydraulic actuator in 10 kN increments until failure. The load-deflection response was monitored, and the failure mode was identified.

3.5.2 Combination of Gravity load and Lateral Cyclic displacements

For SC-2, SC-9, and SC-10, a constant gravity load of 75 kN was first applied. Subsequently, lateral cyclic displacements were introduced using a horizontal hydraulic actuator with 250 kN capacity. The displacement history followed the ACI 374 protocol, as demonstrated in Fig. 5. This was done through a 1st order of analysis, with increasing drift ratios converted to physical displacements based on the 500 mm column height. Loading continued until severe degradation or punching shear failure occurred.

All specimens were simply supported along all four edges to simulate practical boundary conditions representative of actual structural systems, with constraints applied to prevent uplift and out-of-plane movement.

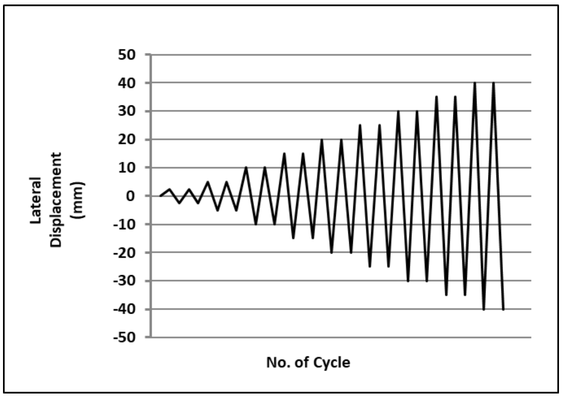

Figure 5. ACI 374 Cyclic loading protocol used [22]

4. Results and Discussion

4.1 Mechanical Characteristics of Hardened Concrete

To better understand the structural performance of the tested elements, the mechanical characteristics of the concrete utilized in casting the specimens were thoroughly assessed. The following tests were performed: Compressive strength tests (cubes and cylinders). The splitting tensile strength was determined through testing following ASTM C496 [27]. Flexural strength test was performed under ASTM C78 [28]. The modulus of elasticity was evaluated following the procedures outlined in ASTM C469 [29]. The summary of test results is shown in Table 5. All values in this table are the mean of three specimens cured in water for 28 days.

Table 5. Summary of the Hardened Concrete Properties

fcu (MPa)	$f'c$ (MPa)	ft (MPa)	fr (MPa)	Ec (MPa)	Dry Density (kg/m3)
40.6	31.3	3.2	3.41	27564	2417

fcu : cubic compressive strength of concrete
$f'c$: Cylinder compressive strength of concrete
ft : Splitting tensile strength
fr : Modulus of rupture
Ec : Static modulus of elasticity

4.2 Test under Gravity Load Only

Specimen SC-G was loaded monotonically with an increasing vertical force applied at the column's top surface until structural failure occurred. The test outcome is presented in Table 6. The ultimate load recorded from this specimen served as a reference for evaluating the performance of all other specimens. To assess the structural performance and validate the effectiveness of the loading setup, the tests were conducted under vertical loading conditions by applying 60% of SC-G's ultimate load to the remaining specimens. The loading capacity of the specimen SC-G was determined to be 124.64 kN, and the maximum deflection was found to be 16.63 mm. This deflection is the maximum displacement recorded from the specimen. The relationships of gravity load compared to slab deflection at mid-span and one-third-span length are displayed in Fig. 6.

Table 6. Test Results of Control Specimen (SC-G)

Specimen Name	First crack load (kN)	Def. at first crack (mm)	Ult. Load Pu (kN)	Def. at ultimate load Δu (mm)	Strain in steel at ultimate load (mm/mm)
SC-G	25	1.8	124.6	16.63	0.002064

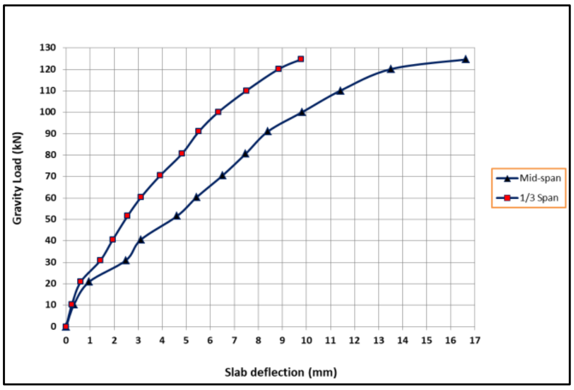

Figure 6. Load–Deflection Relationship under Gravity Loading for Specimen SC-G

The result showed that the specimen of slab-column connection had a very high initial stiffness from the beginning stage of the application of load. However, after reaching 30% of the ultimate capacity or the first visible crack was obtained, the development of stiffness started to decline. The strain in the slab was measured at the position of maximum bending moment at mid-slab under the column. Two strain gauges were affixed to the flexural reinforcement in each direction to monitor strain development, and the average readings were recorded for analysis. Two additional strain gauges were installed on the main longitudinal reinforcement bars within the column to assess stress distribution at the slab-column interface, which significantly influences the overall behavior of the structure. Figure 7 shows the load-strain relationship of the flexural reinforcement of the slab.

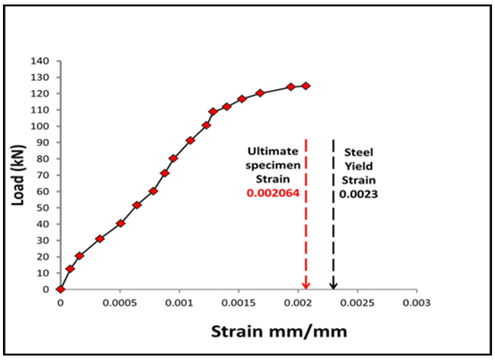

Figure 7. Load-strain curve in flexural slab reinforcement

For comparison purposes, the load–strain response of the flexural reinforcement in the reference specimen (SC-G) indicated that a strain of 0.002064 was recorded at the ultimate applied load of 124.64 kN. The experimental yield strain of the steel reinforcement was equal to 0.0023, This strain value, being lower than the yield strain of the reinforcement, indicates that the failure mode was governed by pure punching shear. During the loading process, several longitudinal cracks developed on the tension face of the slab. Also, transverse cracks of the tension surface emerged around the column area. A non-uniform circular shear crack developed in the tension zone of the slab at the stage of structural failure. In terms of compression, the column pushed through the slab without any visible cracking, indicating that failure was governed by shear rather than flexural mechanisms. Figure 8 shows the crack patterns observed on the upper and lower surfaces of the specimen.

Figure 8. Crack Patterns Observed in Specimen SC-G on Bottom and Top Slab Surfaces

4.3 Tests with Horizontal Displacement

This evaluation was performed using a load combination in which a gravity load was applied on the upper section of the column surface. In contrast, lateral cyclic movements were applied consistently at the section furthest away from the base using a displacement control system for the ACI 374 loading protocol. The results of the cyclic loading tests for all specimens are summarized in Table 7. Figure 9 depicts cyclic curves showing the relation of lateral force against lateral displacement.

Table 7. Cyclic Loading Test Results of Specimens

Specimen	Ultimate lateral load (kN)	Ultimate lateral displacement (mm)	Mid-span deflection after gravity load application (mm)	Mid-span deflection at failure (mm)	Lateral load corresponding to ultimate displacement (kN)
SC-9	+32.4, -32.2	+40, -40	8.69	13.41	+7.2, -7.3
SC-10	+46.3, -45.5	+20, -20	5.25	6.33	+25.7, -24.3
SC-2	+28.6, -25.3	+35, -35	8.16	12.52	+8.8, -7.5

The comparison among these figures indicates that the shape of the column (circular) and reinforcement (spiral) in SC-9 produces a comparatively higher ultimate load, stiffness, and ductility than SC-2 of the square column and tied reinforcement. The ultimate lateral load increase summary was +13.3%, -26.1%. The final lateral displacement determined that SC-9 was (±40 mm) and SC-2 was (±35 mm). As for specimen SC-10, adding a column capital increased the rigidity and ultimate load of the connection by strengthening the connection's ability to resist lateral forces. Compared to the square column, there is a significant improvement in the ultimate lateral load and drift ratio, which shows the effectiveness of the solution with a circular spiral column used in the lateral cyclic loading case.

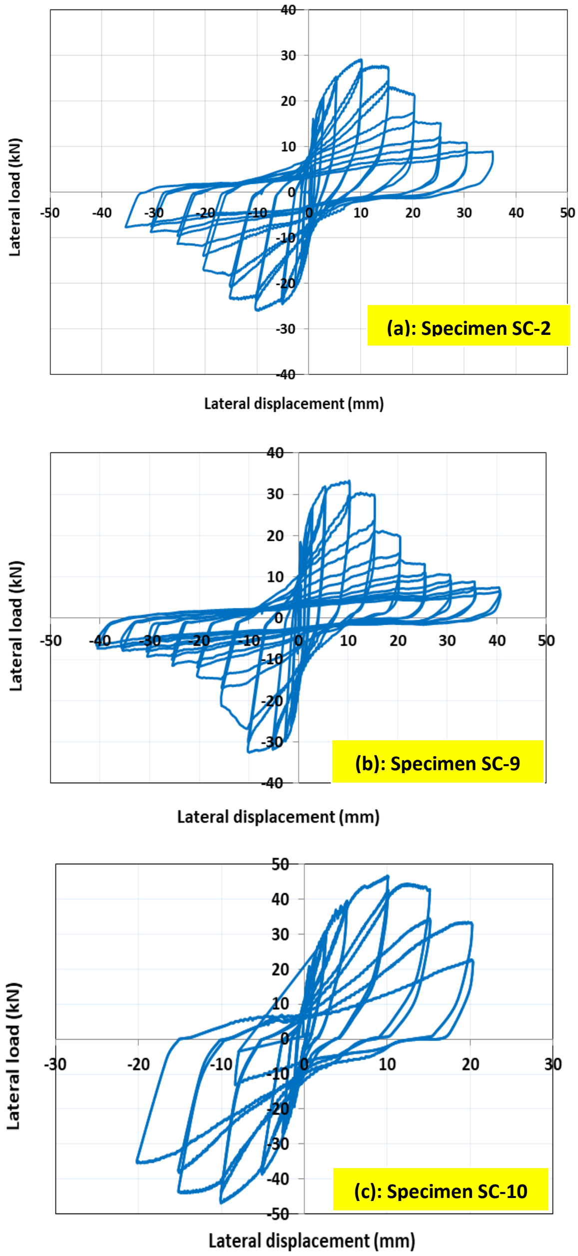

Figure 9. Lateral Load–Displacement Relationships for the Tested Specimens

The comparison of SC-9 and SC-10 shows that circular columns with column capitals influence under cyclic loading. In contrast, comparing SC-10 and SC-2 shows that circular spiral columns with column capitals are significantly better than those between square-tied columns. The ultimate load of SC-10 has been much greater than that of SC-9 by about (±39 %). Maximum lateral displacement for SC-9 was (±40 mm) and (±20 mm) for SC-10. These values show that SC-9 had greater ductility and energy dissipation but lower ultimate load and stiffness than SC-10. The presence of circular spiral columns with column capital n slab-column connections led to a noticeable increase in ultimate lateral load by about +62%, -80%.

4.3.1 Influence of Gravity Load Only and Combined Loading

Figure 10 illustrates the relationship between the applied vertical gravity load and mid-span deflection under two distinct loading conditions: gravity-only and combined gravity with lateral cyclic displacement. This comparison is crucial for evaluating the influence of combined loading on the structural performance of slab-column connections, particularly when enhanced with spiral reinforcement and column capitals.

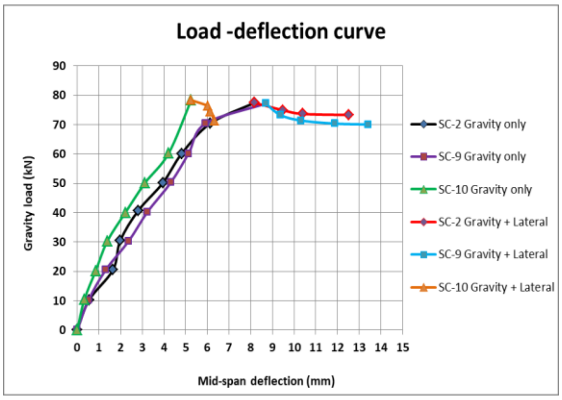

Figure 10. Gravity load vs slab deflection at each loading stage

Ultimate deflections of SC-2 and SC-9 at the end of loading were about 12.5 mm and 13.4 mm, respectively, which makes the SC-9 slightly have a larger ultimate displacement, due to reinforced (spiral) and column cross-section with a circular size, which improved. In contrast, SC-10 under combined loading significantly reduces its ultimate deflection to just 6.32 mm. This decrement is related to the use of the column capital that increases the connection stiffness and restrains the deformation of the slab-column system under large loads. The ultimate load-carrying capacity is increased for SC-2 and SC-9, especially for the combined loading scenarios, and ductility, expressed as the ability to support high deflections before failure, is considerably greater. Concerning stiffness, SC-10 exhibits the best stiffness, reflected by its lowest deflection values under both gravity load alone (5.25 mm) and combined loading (6.32 mm). The column capital creates more stiffness in the connection region, effectively diminishing mid-span deflections. Figure 11 illustrates the relationship between the gravity load applied and the ultimate strain in the slab reinforcement.

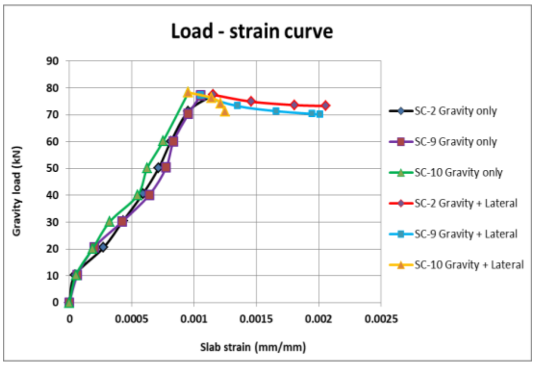

Figure 11. Gravity load vs slab strain at each loading stage

This figure shows that SC-10 showed the highest stiffness compared with SC-9 and SC-2 under the gravity load only in the initial loading stage. The specimen SC-10 has a steeper curve up to the desired gravity, corresponding to a strain of approximately 0.001 mm/mm. This means SC-10 could overcome deformation more than the other specimens under the same loading conditions. However, the same was not observed under lateral cyclic loading, especially in the approach to failure. The strain for SC-10 at failure was 0.00124 mm/mm, which is lower than that observed for SC-9 and SC-2 at failure, which were 0.002 mm/mm and 0.0021 mm/mm, respectively.

4.3.2 Crack Patterns and Observed Failure Modes

First visible cracks were generally observed at gravity loads of 20 kN and 30 kN, respectively. These cracks started in the slab beneath the column corner under the gravity load. This indicates that all specimens crack initially under the gravity load stage. Fine flexural cracks commence with the early application of gravity loads on the tension face of the slab, mainly around the column periphery. It was also observed that the crack propagation and failure mode of the circular column and spiral reinforcement for specimen SC-9 were similar to those of the reference specimen SC-2. The failure type was punching shear, but there was also the fact that the column was less vulnerable to lateral actions. In contrast, the contribution of the column capital in controlling the growth of cracks and failure pattern appeared through (SC-10), which is very clearly and significantly measurable through crack growth. Figure 12 shows the pattern of cracks and mode of failure at the end of testing. For this figure, markings attempt to differentiate cracks in "lateral" effects (red) versus "gravity" or vertical load (blue, black).

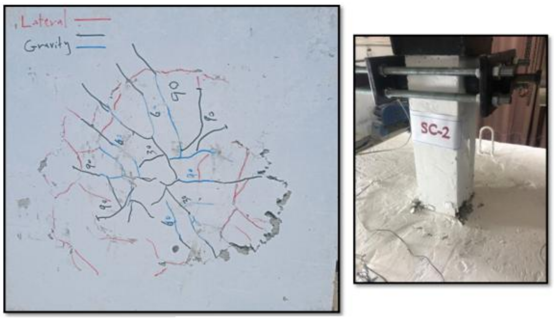

(a): Specimen SC-2

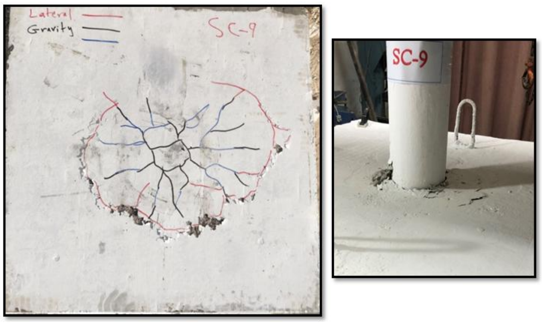

(b): Specimen SC-9

(c): Specimen SC-10

Figure 12. Crack Patterns and Failure Modes on the Compression and Tension Faces of All Tested Specimens

4.3.3 Stiffness, Ductility, and Energy Dissipation Characteristics of Slab-Column Connections

Stiffness, energy dissipation capacity, and ductility of the R.C connections are operators for the structural frame subjected to seismic effects represented by the combined gravity loads and lateral cyclic displacements. They are essential factors for the overall seismic performance of a structure. For moderate lateral deformations, the connection preserves a relatively high stiffness, primarily owing to the flexural rigidity of the slab and the confinement around the column. When the deformations are further pronounced, cracks are formed, and the steel reinforcement yields, decreasing the stiffness, enabling plastic deformations and increasing ductility, preventing sudden brittle failure. For lateral load vs. lateral displacement, the backbone curves of hysteresis curves are given in Fig. 13. The backbone curve (also called an envelope curve) of structural members' force-deformation (or moment-rotation) response can be simplified using cyclic tests. Hysteresis loops can be complex features, including strength degradation and stiffness degradation when structures are subjected to cycles of reversed loading. To capture the essential nonlinear characteristics, without the majority of the complexity in full hysteresis loops, researchers often extract the peak points from each cycle of the hysteresis loops to construct an "envelope" curve representing the maximum structural response. This curve is commonly referred to as the backbone curve [30].

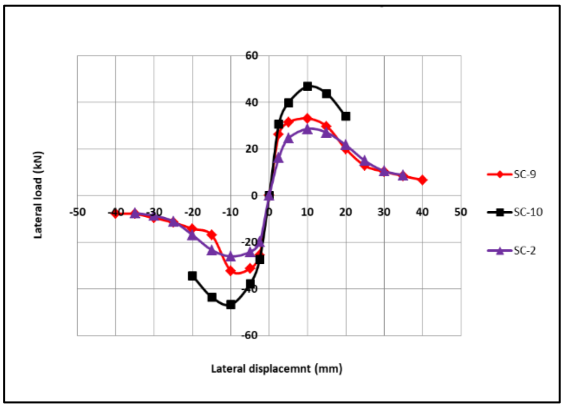

Figure 13. Backbone Curves of Lateral Load–Displacement Relationships

The backbone curve is an integral concept in investigating and modeling the inelasticity of slab-column connections under cyclic lateral loading. It gives a direct, simplified description of how these connections fail and how large their deformability and ductility are expected to be before collapse. It summarizes the key response features from initial stiffness via peak strength, to post-peak degradation [31].

The stiffness of slab-column connections plays a critical role in maintaining the overall lateral stability of reinforced concrete floor systems. These joints must effectively transfer significant shear forces and bending moments from the slab to the supporting columns under both gravity and cyclic lateral loads [32]. Following the onset of initial cracking, a progressive reduction in stiffness is typically observed, primarily due to crack propagation and bond deterioration around the reinforcement. This deterioration leads to a gradual decline in load-bearing capacity with each subsequent loading cycle.

Figure 14 illustrates the peak-to-peak stiffness values obtained for each loading cycle, which were derived from the backbone curves shown in Figure 11. The stiffness for each cycle was determined by relating the ultimate lateral load to the corresponding displacement. The results revealed a rapid decrease in stiffness as cyclic loading progressed. Notably, a pronounced softening effect was observed after the second cycle for each pair of cycles at a constant amplitude.

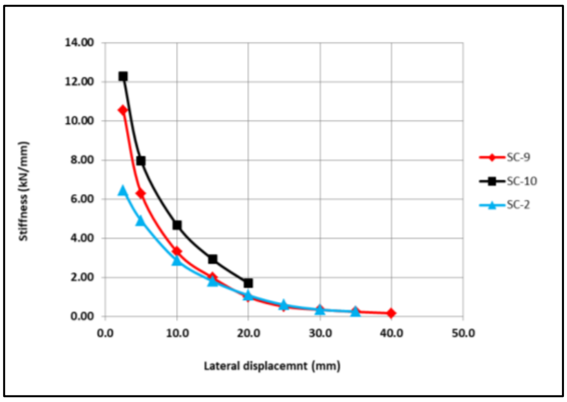

Figure 14. Backbone Curves of Lateral Load–Displacement Response

Table 8. summarizes the ultimate stiffness, ductility indices, and energy dissipation capacities for all tested specimens.

Table 8. Stiffness, Ductility, and Energy Dissipation of the Tested Specimens

Specimen Name	Ultimate Stiffness (kN/mm)	Ductility Index %	Energy Dissipation (kN.mm)
SC-2	6.45	1.92	1232
SC-9	10.52	3.7	1434
SC-10	12.27	3.38	1511

5. Conclusions

Based on the experimental outcomes and comparative performance of the tested slab-column specimens under gravity and lateral cyclic loading, the following conclusions are drawn:

1- specimens with circular spiral columns exhibited enhanced lateral load capacity and improved hysteretic response compared to square-column specimens. The more uniform stress distribution in circular sections led to increased ductility and more stable energy dissipation under cyclic loads.

2- Incorporation of a column capital led to significantly increased in the punching shear resistance and lateral stiffness of the connection. SC-10 showed the highest ultimate stiffness (12.27 kN/mm) and the lowest mid-span deflection under combined loading, highlighting the effectiveness of geometric enhancement in seismic design.

3- Spiral reinforcement and circular geometry in SC-9 enhanced the energy dissipation capacity (1434 kN·mm) and ductility index (3.7) compared to square-tied reinforcement in SC-2. However, SC-10, while exhibiting lower ductility than SC-9, achieved the highest energy dissipation (1511 kN·mm).

4- All specimens experienced progressive stiffness degradation with increased displacement cycles. However, SC-10 maintained superior stiffness due to the combined effect of spiral confinement and the column capital, which delayed the onset of severe cracking and structural softening.

5- The circular column with spiral reinforcement (SC-9) showed theoretically superior performance due to improved confinement and stress distribution, resulting in higher ductility and increased lateral displacement.

6- According to theoretical evaluations, adding a column capital in SC-10 significantly enhanced punching shear resistance and lateral stiffness. However, this enhancement reduced ductility, highlighting a theoretical trade-off between stiffness and deformability.

7- The theoretical analyses indicate that the combined geometric and reinforcement enhancements in SC-10 substantially increased ultimate lateral load capacity and overall structural rigidity, though at the expense of reduced ductility and displacement capacity.

6. Recommendations and Limitations

6.1. Recommendations:

Based on the findings of this study, the following recommendations are proposed for improving the seismic performance of reinforced concrete flat slab-column joints:

1. Use of Circular Columns with Spiral Reinforcement: Circular cross-sections combined with spiral confinement enhance ductility, energy dissipation, and lateral load capacity, and are recommended for structures in seismic regions.
2. Incorporation of Column Capitals: Adding column capitals significantly improves punching shear resistance and lateral stiffness. Their use is especially beneficial in structures where minimizing drift and enhancing integrity under cyclic loads is critical.
3. Design for Equivalent Flexural Stiffness: When comparing or designing slab-column systems with different column geometries, maintaining equivalent flexural stiffness ensures structural fairness and helps isolate the effects of geometry on performance.
4. Further Development of Seismic Detailing: Reinforcement detailing—particularly lateral confinement and connection zones—should follow enhanced seismic standards (e.g., ACI 318, ACI 374) to delay degradation and cracking under repeated lateral cycles.

6.2. Limitations:

While the experimental results provide valuable insights, several limitations are considered:
1. Scale Effect: The specimens were constructed at a 1:2.5 scale. Although care was taken to maintain realistic behavior, full-scale structures may exhibit additional complexity.
2. Limited Number of Specimens: The study focused on four configurations, limiting the results' generalizability. More specimens and variable configurations would improve statistical confidence.
3. Lack of Numerical Validation: Although an analytical comparison was introduced, a complete finite element analysis would provide deeper insight and validate experimental observations.
4. Material Variability and Durability: Only normal-strength concrete was tested. Future research should evaluate high-strength or fiber-reinforced mixes and long-term effects like fatigue or corrosion resistance.
5. Boundary Conditions: The simply supported test setup may not perfectly simulate in-situ boundary conditions in real buildings. Investigating different support restraints could offer further insights.

7. References

[1] H. N. G. Al-Maliki, A. Al-Balhawi, and A. M. Ali, "Punching shear resistance of reinforced concrete flat slabs strengthened by CFRP and GFRP: A review of literature," Eng. Technol. J., vol. 39, no. 8, pp. 1281-1290, 2021. https://doi.org/10.30684/etj.v39i8.2011

[2] A. S. Genikomsou, "Seismic damage assessment of reinforced concrete slab-column connections: Review of test data, code provisions and analytical models," Buildings, vol. 14, no. 2, p. 465, Feb. 2024. https://doi.org/10.3390/buildings14020465

[3] S. Agudze, D. K. Amoah, and B. K. Sasraku-Neequaye, "Comparative study of RCC flat slab and RCC beam-and-slab floor systems," Civil Environ. Res., vol. 10, no. 8, pp. 17-26, 2018.

[4] R. Z. Alrousan and B. R. Alnemrawi, "Punching shear behavior of FRP reinforced concrete slabs under different opening configurations and loading conditions," Case Stud. Constr. Mater., vol. 17, e01508, Dec. 2022. https://doi.org/10.1016/j.cscm.2022.e01508

[5] ACI Committee 318, Building Code Requirements for Structural Concrete (ACI 318-19) and Commentary. Farmington Hills, MI, USA: ACI, 2019.

[6] European Committee for Standardization, Eurocode 2: Design of Concrete Structures - Part 1-1: General Rules and Rules for Buildings (EN 1992-1-1). Brussels, Belgium: CEN, 2004.

[7] Canadian Standards Association, Design of Concrete Structures (CSA A23.3-19). Toronto, ON, Canada: CSA Group, 2019.

[8] JSCE, Standard Specifications for Concrete Structures - 2007: Design. Tokyo, Japan: Japan Soc. Civil Eng., 2007.

[9] E. Yehia, A. H. Khalil, E.-E. Mostafa, and M. A. El-Nazzer, "Experimental and numerical investigation on punching behavior of ultra-high performance concrete flat slabs," Ain Shams Eng. J., vol. 14, no. 10, 102208, Oct. 2023. https://doi.org/10.1016/j.asej.2023.102208

[10] Applied Technology Council, Effects of Strength and Stiffness Degradation on Seismic Response, FEMA P440A. Washington, D.C., USA: FEMA, Jun. 2009.

[11] M. Tonidis, A. Sharma, and V. Birtel, "Experimental and numerical investigations on the influence of transverse beams and slab on the seismic behavior of non-seismically designed exterior beam-column joints," Earthq. Eng. Struct. Dyn., vol. 53, no. 14, pp. 4451-4476, Sep. 2024. https://doi.org/10.1002/eqe.4228

[12] T.-K. Lee and C.-C. Chen, "Seismic investigation of reinforced concrete columns with different transverse reinforcements," Adv. Struct. Eng., vol. 25, no. 4, Jul. 2022. https://doi.org/10.1177/13694332221114071

[13] B. Isufi, M. Rossi, and A. P. Ramos, "Influence of flexural reinforcement on the seismic performance of flat slab-column connections," Eng. Struct., vol. 242, 112583, Sep. 2021. https://doi.org/10.1016/j.engstruct.2021.112583

[14] G. T. Truong, K. K. Choi, and C. S. Kim, "Punching shear strength of interior concrete slab-column connections reinforced with FRP flexural and shear reinforcement," J. Build. Eng., vol. 46, 103692, 2022. https://doi.org/10.1016/j.jobe.2021.103692

[15] I. A. Sarhan, A. S. Mahmoud, and M. A. Hussian, "Punching shear resistance of high-strength GFRP reinforced concrete flat slabs," Iraqi J. Civil Eng., vol. 11, no. 1, pp. 72-93, 2017. https://doi.org/10.37650/ijce.2017.134052

[16] A. R. Yousif, A. S. Mahmoud, and M. T. Abduljaleel, "Punching strength of GFRP reinforced concrete slab-column connections with openings by the finite element method," ZANCO J. Pure Appl. Sci., vol. 28, no. 6, pp. 56-67, 2017. https://doi.org/10.21271/ZJPAS.28.6.8

[17] M. Zhou and T. D. Hrynyk, "Numerical investigation on the structural performance of post-tensioned precast concrete two-way slab-column connections," Structures, vol. 69,

107520, Nov. 2024. https://doi.org/10.1016/j.istruc.2024.107520
[18] Y. Jia and J. C. L. Chiang, "Finite element analysis of punching shear of reinforced concrete mushroom slab-column connections using ABAQUS," in Advances in Frontier Research on Engineering Structures, Y. Yang, Ed. Lecture Notes in Civil Engineering, vol. 286. Springer, 2023. https://doi.org/10.1007/978-981-19-8657-4_8
[19] R. B. Babu and R. Thenmozhi, "Experimental and numerical studies on punching shear strength of concrete slabs containing sintered fly ash aggregates," Rev. Constr., vol. 20, no. 1, pp. 15-24, 2021. https://doi.org/10.7764/RDLC.20.1.15
[20] S. Rafiee, A. Hosseini, and M. S. Marefat, "Seismic details for exterior connections of post-tensioned flat slabs to steel columns using steel plates, vertical stiffeners and bolts," J. Build. Eng., vol. 36, 102140, Apr. 2021. https://doi.org/10.1016/j.jobe.2020.102140
[21] S. Rafiee and M. S. Marefat, "Experimental and numerical evaluation of new seismic details for connection of post-tensioned flat slabs to edge steel columns," Curr. Trends Civil Struct. Eng., vol. 6, no. 4, pp. 1-11, Nov.
[22] ACI Committee 374, Acceptance Criteria for Moment Frames Based on Structural Testing and Commentary (ACI 374.1-05). Farmington Hills, MI, USA: ACI, 2005.
[23] Sika Group, Technical Data Sheet: Sika® ViscoCrete®-180 GS - High-Performance Superplasticizer. Baar, Switzerland: Sika Services AG.
[24] ASTM International, ASTM A615/A615M-20: Standard Specification for Deformed and Plain Carbon-Steel Bars for Concrete Reinforcement. West Conshohocken, PA, USA: ASTM Int., 2020.
[25] I.Q.S, Aggregate from Natural Sources for Concrete and Construction, Iraqi Specification No. 45. Baghdad, Iraq: COSQC, 2019.
[26] ACI Committee 308, Guide to External Curing of Concrete, ACI 308R-16. Farmington Hills, MI, USA: ACI, 2016.
[27] ASTM International, ASTM C496/C496M-17: Standard Test Method for Splitting Tensile Strength of Cylindrical Concrete Specimens. West Conshohocken, PA, USA: ASTM Int., 2017.
[28] ASTM International, ASTM C78/C78M-18: Standard Test Method for Flexural Strength of Concrete (Using Simple Beam with Third-Point Loading). West Conshohocken, PA, USA: ASTM Int., 2018.
[29] ASTM International, ASTM C469/C469M-14: Standard Test Method for Static Modulus of Elasticity and Poisson's Ratio of Concrete in Compression. West Conshohocken, PA, USA: ASTM Int., 2014.
[30] C. S. Lee and S. W. Han, "An accurate numerical model simulating hysteretic behavior of reinforced concrete columns irrespective of types of loading protocols," Int. J. Concr. Struct. Mater., vol. 15, no. 1, Dec. 2021. https://doi.org/10.1186/s40069-020-00446-5
[31] I. N. Robertson and G. P. Johnson, "Cyclic lateral loading of non-ductile slab-column connections," ACI Struct. J., vol. 103, no. 3, pp. 356-364, Jun. 2006. https://doi.org/10.14359/15313
[32] M. Ahmed, "Strengthening of reinforced concrete slab-column connections using CFRP," presented at the 2nd Conf. Civil Eng., Khartoum, Sudan, Dec. 2018.